# Accepted Manuscript

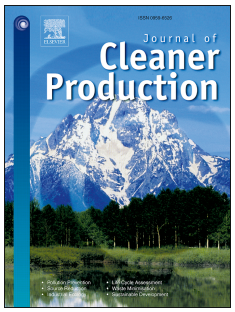


Removal of Cu(II), Cd(II) and Pb(II) ions from aqueous solutions by biochars derived from potassium-rich biomass

Zahoor Ahmad, Bin Gao, Ahmed Mosa, Haowei Yu, Xianqiang Yin, Asaad Bashir, Hossein Ghoveisi, Shengsen Wang

PII: S0959-6526(18)30155-0

DOI: 10.1016/j.jclepro.2018.01.133

Reference: JCLP 11813

To appear in: *Journal of Cleaner Production*

Received Date: 19 March 2017

Revised Date: 19 November 2017

Accepted Date: 17 January 2018

Please cite this article as: Ahmad Z, Gao B, Mosa A, Yu H, Yin X, Bashir A, Ghoveisi H, Wang S, Removal of Cu(II), Cd(II) and Pb(II) ions from aqueous solutions by biochars derived from potassium-rich biomass, *Journal of Cleaner Production* (2018), doi: 10.1016/j.jclepro.2018.01.133.

[Amount of words = 9081]

# Removal of Cu(II), Cd(II) and Pb(II) ions from aqueous solutions by biochars derived from potassium-rich biomass

Zahoor Ahmad[a,b*], Bin Gao[b*], Ahmed Mosa[c, b], Haowei Yu[d, b], Xianqiang Yin[e, b], Asaad Bashir[f, b], Hossein Ghoveisi[b], Shengsen Wang[b]

[a] Department of Agricultural Sciences, University of Haripur, Haripur, Khyber Pakhtunkhwa, Pakistan

[b] Department of Agricultural and Biological Engineering, University of Florida, Gainesville, FL 32611, United States

[c] Soils Department, Faculty of Agriculture, Mansoura University, 35516 Mansoura, Egypt

[d] College of Horticulture, Sichuan Agricultural University, Chengdu, Sichuan, 611130, China

[e] College of Natural Resources and Environment, Northwest A&F University, Yangling, Shaanxi, 712100, China

[f] Institute of Soil and Environmental Sciences, University of Agriculture, Faisalabad, Pakistan

[*]Corresponding authors. Tel.: +92 (0) 995 615272; +1 (352) 392-1864 ext. 285

E-mail address: zahoorahmad@uoh.edu.pk; bg55@ufl.edu

**Abstract:**

This work evaluated the novel application of biochars derived from potassium (K)-rich feedstock (banana peels (BB) and cauliflower leaves (CB)). The sorptive property of the produced biochars was evaluated under multi-element [Copper (Cu(II)), Cadmium (Cd(II)) and Led (Pb(II))] sorption experiments. Morphologies of the pre- and post-sorption samples were characterized using SEM/EDS and XRD spectra analyses. The produced biochar was further subjected to mono-element sorption studies to explore the effect of the pH value of the sorbate solution on the removal efficiency of Cu(II), Cd(II) and Pb(II) ions. Biochar productivity was noticeably high (61.44 and 64.66% for BB and CB, respectively) due to the catalytic action of K during the pyrolytic conversion of the feedstock. K-minerals were the predominant on the XRD patterns of both biochars. Metal sorption capacity of BB was much greater than that of CB due to its higher electrostatic attraction, which was the predominant mechanism governed sorption process. Sorption of metal ions onto BB and CB was pH-dependent as the sorption capacity increased significantly with the increase of the pH value of sorbate solutions (6.0 with Cu(II), Pb(II) and 8.0 with Cd(II)). Dynamics of metal ions sorption onto biochars showed competitive sorption following the order: Pb(II) > Cu(II) > Cd(II).

**Keywords:** Vegetable biomass; food residuals; engineered biochar; potassium-rick feedstock; environmental remediation

## 1. Introduction

Unlike other anthropogenic-based pollutants, heavy metals are not degradable and show a high tendency toward reaching the food chain (Wuana and Okieimen, 2011). Aquatic environments, especially rivers (Ali et al., 2016; Gao et al., 2015; Varol and Şen, 2012) and groundwater (Chen et al., 2016; Nouri et al., 2008) are the primary transport medium for these metals. Therefore, more emphasis is being placed for the treatment of contaminated aqueous solutions before reaching water reservoirs. Classical treatments technologies of heavy metals decontamination such as bioremediation (Zeraatkar et al., 2016), chemical precipitation (Fu et al., 2012), electrocoagulation (Al-Shannag et al., 2015), ion exchange resin (Edebali and Pehlivan, 2016), membrane separation (Hebbar et al., 2016), adsorption (Hua et al., 2012; Inyang et al., 2016), photoreduction (Chowdhury et al., 2017), reduction (Li et al., 2015), reverse osmosis (Li et al., 2015), and solvent extraction (Ye et al., 2015) have been widely investigated on aqueous solutions. These methods have their own advantages and disadvantages; however, most of them are extremely expensive and inefficient at large quantities (Mosa et al., 2011) .

In the last decade, attention has been drawn toward using biochar for wastewater decontamination based on its cost-efficiency, simple processing and eco-friendly. Biochar is a charcoal-like material derived from the thermal processing (e.g., pyrolysis) of carbon-rich biomass (e.g. agricultural byproducts) under oxygen-limited conditions (Inyang et al., 2016). Unlike conventional feedstock-processing technologies (e.g. combustion), pyrolysis based-biochar is green (environmentally friendly), carbon-negative (it stores carbon in the form of stable charcoal) and produces flammable gases and liquids (e.g. syngas) (Lehmann, 2007). Biochar has been credited with multiple environmental benefits due to its high resistance against microbial decay, and its high sorption capacity of ions and molecules. In spite of its widespread

application in different fields including soil quality enhancement (Chen et al., 2017; Suliman et al., 2017) and carbon sequestration (Creamer et al., 2016; Creamer et al., 2014), biochar and its derivatives (e.g. biofilters) had been intensively investigated for wastewater decontamination (Ding et al., 2016b; Inyang et al., 2014; Mosa et al., 2016).

Several feedstock materials had been investigated for biochar production. Among them, agricultural byproducts, e.g. rice husk (Xu et al., 2013a), wheat straw (Xue et al., 2016), sugarcane bagasse (Ding et al., 2014), tomato leaves (Yao et al., 2013), peanut hull (Xue et al., 2012) and cotton wood (Zhang et al., 2012) were the most widely engineered biomass. However, there remains a great deal of uncertainty with respect to the sorption capacity of pristine biochar as compared with other conventional biosorbents (e.g. activated carbon). Biochar activation, therefore, is of great interest to improve the remediation efficacy of the pristine biochar. Among several activation methods i.e. (1) mechanical activation (e.g. ball milling), (2) physical activation (e.g. steam activation and gas purging), (3) impregnation with natural minerals (e.g. clay minerals and mineral oxides), and (4) magnetic modification, chemical modification of biochar (e.g. acid/base treatment, organic solvents treatment, coating, and surfactant modification) received much more attention due to its high efficiency toward biochar activation (Rajapaksha et al., 2016). Chemical activation with potassium-based compounds (e.g. KOH and $K_2CO_3$) is one of the most widely used chemical modification methods for increasing total surface area, porosity and active functional groups of the pristine biochar (Dehkhoda et al., 2016; Jin et al., 2016; Yu et al., 2016). Furthermore, there are recent reports highlighting its significant catalytic effect during pyrolysis through lowering the initial pyrolysis restraining the formation of volatile compounds; thus, decrease the weight loss rate and increase the biochar yield (Hao et al., 2015; Nowakowski and Jones, 2008). However, there are several drawbacks arise

surrounding chemical activation process including the excessive use of chemical compounds involved in impregnation, neutralization and drying during or after pyrolysis process. This excessive use of chemicals is associated with extra laborious washing and recovery steps during activation process. This will lead to generate huge amounts of hazardous chemical sludge, where its disposal is mostly expensive and non eco-friendly. Consequently, attention has been directed toward considering the chemical constitution of biomass as a crucial factor for biochar production. A promising approach, mainly focusing on the exploitation of potassium-rich biomaterials for the in-situ-self-activation of biochar, is recently highlighted (Chen et al., 2012). The scientific hypothesis of this approach depends mainly on the inherent existence of potassium-rich compounds in the feedstock (e.g. banana peel and cauliflower leaves), which act as in-situ chemical activators during pyrolysis process.

Banana peel and cauliflower leaves are among the most highly produced wastes during cultivation and industrialization of banana and cauliflower food chain. Most of these wastes are usually disposed through landfilling or stockpiling, where they are inappropriate to feed livestock. These disposal systems, however, would lead to tremendous environmental hazards due to their abundance of organic matter and moisture contents (Xu et al., 2017). On the other hand, these wastes are scarce considered as feedstock for biochar production. Probably, due to their high moisture content. Therefore, there is an urgent need to optimize biochar production through the thermal carbonization of these wastes due to their rich-potassium content. Besides, banana peel and cauliflower leaves contain abundant amounts of lignin, cellulose, hemicellulose, pectins, starch, proteins and other phenolic compounds, which favored the formation active functional groups on biochar surfaces (Branca and Di Blasi, 2015; Huynh et al., 2016). This will lead to maximize the sorption capacity of heavy metal ions onto biochar.

The objectives of this study were as follows: (1) studying the effect of the inherent high potassium content of organic feedstock on biochar productivity and characteristics, (2) exploring kinetic and isotherm models of the produced biochar under multi-element sorption experiments (Cu(II), Cd(II) and Pb(II)), (3) investigating the underlying mechanisms contributed in sorption of metal ions onto biochars, (4) studying the effect of pH value of the sorbate solution on sorption capacity of the produced biochars under mono-element sorption experiments, and (5) evaluating the competence of Cu(II), Cd(II) and Pb(II) ions toward sorption onto the produced biochars.

## 2. Materials and methods

### 2.1. Chemical reagents

All chemicals of analytical-reagent grade including $Cu(NO_3)_2.3H_2O$, $Cd(NO_3)_2.4H_2O$, $Pb(NO_3)_2$, NaOH, HCl, $H_2O_2$, and $NaNO_3$ were purchased from Fisher Scientific. Chemical solutions were prepared with Deionized (DI) water (18 MΩ cm).

### 2.2. Biochar preparation

Banana peels and cauliflower leaves were chopped to about 2-cm length, and oven dried at 70 ± 5.0 $^{o}$C for 48 h until reaching weight constant. About 25-30 g of the dry sample was loaded in tubular quartz reactors (6 cm diameter × 28 cm length glass cylinders), and inserted into a bench-top furnace (GSL-1100X, MTI Corporation). Feedstock was converted into biochar through slow pyrolysis at 600 $^{o}$C for 2 h (Inyang et al., 2010; Inyang et al., 2012; Xiao et al., 2017), purged with $N_2$ gas (10 psi). The furnace temperature was raised to 200$^{o}$C, and kept constant for 1 h. Thereafter, temperature was increased at a rate of 15 °C $min^{-1}$ till reaching 600 °C, where it was kept constant for 2 h. Collected biochars were crushed and sieved to obtain the uniform 0.452-1 mm-sized fraction.

### 2.3. Biochar characterization

Samples were analyzed for carbon (C), hydrogen (H), and nitrogen (N) determination using a CHN Elemental Analyzer (Carlo-Erba NA-1500). Total inorganic elements of biochar was determined using inductively coupled plasma optical emission spectrometer (ICP–OES, Perkin Elmer Optima 2100 DV) after the modified dry-ashing method (Enders and Lehmann, 2012). The pH value of biochar was measured in 1:20 (m/v) DI water suspension (Sun et al., 2014). The suspension was stirred for 1 h, and allowed to stand for 5 min before measuring by pH meter (Fisher Scientific Accumet AB250). For measuring zeta potential (ζ), biochar samples were sonicated in DI water following the method described by Johnson et al. (1996), and the charge mobility was quantified on Brookhaven Zeta Plus (Brookhaven Instruments, Holtsville, NY). Specific surface areas of the biochar samples were determined with a Quantachrome Autosorb-1 surface area analyzer. $N_2$ sorption isotherms were measured at 77 K, and interpreted using Brunauer, Emmet, and Teller (BET) theory.

The surface morphology of pre- and post-sorbed biochar samples was investigated by field emission scanning electron microscopy (Nova NanoSEM 450, FEI Company, USA) at 15 kV voltage. Energy Dispersive X-ray Spectroscopy (EDS; AMETEX ) equipped with SEM was used simultaneously to quantify the composition of elements on biochars surface. Post-sorption samples were prepared by shaking biochar with mixture of Cu(II), Cd(II) and Pb(II) (0.2 mM for each) at the rate of **0.5:200 (w:v)** for 24 h at room temperature (22 ± 0.5 $^{o}$C). Post-sorption samples were filtered through 0.25 μm pore size nylon membrane filters (GE cellulose nylon membrane), washed three times with DI water, and oven-dried at 90$^{o}$C for 24 h.

XRD pattern of pre-and post-sorption biochar samples was performed by using a computer-controlled X-ray diffractometer (Philips APD 3720) equipped with a stepping motor and graphite

crystal monochromator. Post-sorption samples were prepared by shaking biochars with either mixture or individual Cu(II), Cd(II) and Pb(II) ions (each at concentration of 0.2 mM) for 24 h at room temperature (22 ± 0.5 $^{o}$C). Samples were washed three times with DI water and oven-dried as stated earlier.

**2.4. Sorption Kinetics and isotherms**

Sorption kinetics of Cu(II), Cd(II) and Pb(II) ions onto BB were determined by shaking 0.5 g of biochar with 200 mL of a mixture containing 200, 200 and 600 mg $L^{-1}$ of Cu(II), Cd(II) and Pb(II) ions, respectively (i.e. 0.5:200 w:v) in acid washed glass bottles, without pH modification. Similarly, 200 mL mixture of Cu(II) (150 mg $L^{-1}$), Cd(II) (200 mg $L^{-1}$) and Pb(II) (200 mg $L^{-1}$) was shaken with 0.5g of CB. All samples contained 0.01 M $NaNO_3$ solution as background electrolyte. Biochar suspensions were shaken at room temperature (22 ± 0.5 $^{o}$C), and samples were withdrawn at different time intervals ranging between 0.25-48 h. Blank corrections were performed without the sorbent material to distinguish between actual sorption mechanisms and possible heavy metals precipitation. Samples were filtrated through 0.25 μm pore size nylon membrane filters (GE cellulose nylon membrane), and metal ions concentration was determined by ICP-OES.

Sorption isotherms were carried out on mixtures having various concentrations of Cu(II) (50-200 mg $L^{-1}$ for BB and CB), Cd(II) (50-500 and 50-350 mg $L^{-1}$ for BB and CB, respectively) and Pb(II) (100-1000 and 100-850 mg $L^{-1}$ for BB and CB, respectively) without any pH modifications. All samples contained 0.01 M $NaNO_3$ solution as background electrolyte. Sorbent and sorbate (0.5:200 w:v) were shaken in polypropylene digestion vessels (Environmental Express**)** following the same procedures of sorption kinetics. Samples were withdrawn at contact time of 24 h.

### 2.5. Effect of the pH value of sorbate solution.

The effect of pH value on sorbent-sorbate interaction was studied under mono-element sorption experiments at concentration of 200 mg $L^{-1}$. By using 0.1 M of either HCL or NaOH, the pH value of sorbates was adjusted according to variations in critical pH values for metal ions sorption (between 2-6 with Cu(II) and Pb(II) sorbates, and between 3-8 with Cd(II) sorbates). BB and CB biochars were mixed with sorbate solutions at the rate of 0.5:200 (w:v), and shaken in digestion vessels for 24 h at room temperature. The pH value of the sorbate solution was readjusted following 2 h from the contact time. Samples were filtered, and the pH value was measured before determination of metal ions concentration. All sorption studies were carried out in duplicates, and additional analyses were performed whenever two measurements showed a difference of more than 5%.

## 3. Results and discussion

### 3.1. Physico-chemical properties of biochars used

Biochar production rate was very high (61.44 and 64.66% for BB and CB, respectively). This low rate of weight losses during pyrolysis (38.56 and 35.34% for BB and CB, respectively) is highlighting the valuable role of the naturally K-rich features of banana peel and cauliflower leaves. The inherent high K content of the organic feedstock might have a catalytic action during its pyrolytic conversion. According to Nowakowski et al. (2007), K impregnation into willow coppice reduced the average pyrolysis energy by about 50 kJ/mol, and enhanced the produced yield of biochar and methane. Another investigation showed a pronounced reduction in the final weight loss of pyrolyzed biomass due to K addition (1.45%/°C *vs.* 2.36%/°C for the impregnated and the untreated biomass, respectively) (Hao et al., 2015).

CNH analyses revealed that both biochars have almost the same amount of C and H contents (Table 1). N content was higher in CB (4.14%) as compared with BB (1.57%). This high content of N in CB could have a functionalization effect on the sorptive properties of CB. Beside its catalytic effect during pyrolysis, the high nitrogen content of CB might act as a precursor for nitrogen-surface functional groups formation and developing the microporous structure of the carbonaceous lattice (Rybarczyk et al., 2015; Zhang et al., 2016).

Elemental analyses of ICP showed biochars with high K content (10.89 and 11.04% for BB and CB, respectively). Calcium concentration was noticeably higher in CB (6.17%) as compared with BB (0.59%). Concentrations of P, Mg, Fe, Zn and Mn were relatively higher in CB as compared with BB. The concentration of Pb(II) was very low in both biochars. Meanwhile, Cu(II) and Cd(II) concentrations were below the detection limit in both biochars.

The pH value of both biochars was very high (10.09 and 10.64 for BB and CB respectively), which reflect their alkaline nature due to the high content of alkaline minerals (K, Ca and Mg). The $N_2$ surface area measurement of BB was relatively low (<5 $m^2 g^{-1}$) as compared with CB (12.5 $m^2 g^{-1}$). Zeta potential (ζ) of both biochar was negative, and BB has more electronegativity (-93.77 mV) as compared to CB (-36 mV).

The relatively low surface area of BB was further confirmed by the SEM micrographs, which showed BB surfaces in a compact rigid structure with smooth flacks (Fig. 1A). On the other hand, CB surfaces appeared in a roughness shape with complicated network of micro-pores and cracks (Fig. 1C). This micro-morphological structure of CB could be the reason of its higher surface area as compared with BB. The high content of K in both biochar was further confirmed by the presented high peaks of K in the EDS spectra (Fig. 1a and 1c). Beside high peaks of K, EDS spectra of both biochars showed the presence of O, Ca, Cl, Si, P, Mg and Na peaks.

Meanwhile, CB showed a high S peak, which was not existed in BB. This could be attributed to the high content of organosulfur compounds existed in cauliflower and other Brassica vegetables (Stoewsand, 1995).

The XRD patterns showed the excellent crystallinity of both biochars (Fig. 2). Based on the high content of K existed in the feedstock, K-minerals were the predominant on the XRD patterns of both biochars. The broad diffraction peaks concentrated approximately between 12° and 66° 2-theta in BB correspond mainly to Kalicinite ($KHCO_3$), monetite ($CaHPO_4$) and sylvite (KCl) (Fig. 2e). The formation of Kalicinite in the carbonized biomass may be derived from $K_2CO_3$ following the exposure to $H_2O$ and $CO_2$ during cooling and storage since $KHCO_3$ would expose to decomposition in temperature higher than 100 $^oC$ (Chen et al., 2012). On the other hand, the elevated background between 28° and 74° 2-theta in CB correspond to sylvite mineral (Fig. 2j). The formation of K-minerals in BB and CB suggested the in-situ-self-activation of biochars during pyrolysis process. This formation of K-minerals during pyrolysis can contribute in sorption process through precipitation onto these minerals or exchanging $K^+$ with other Cu(II), Pb(II) and Cd(II) ions.

**3.3. Sorption Kinetics.**

Both biochars showed almost similar trends in metal ions removal over the contact time (Fig. 3). Apparent sorption was rapid during the first 5-10 h, and the equilibrium was reached at 24 h. Sorption of metal ions onto BB was relatively faster than CB during the initial time of contact. This could be attributed to the higher electronegativity of BB as compared with CB. This kinetic sorption trend matched with most of biochar sorption kinetics, which showed that metal sorption onto biochar is divided into a rapid initial phase during the first initial time of sorption, and another slow phase till equilibrium is reached (Ding et al., 2016a; Shi et al., 2009; Wang et al.,

2015). The early initial sorption phase is dominantly controlled through physisorption force where metal ions are sorbed by the sufficient sorption sites on biochar surfaces. Chemisorption is the dominant force controlling the other slow sorption phase until reaching equilibrium. In this phase, metal ions are sorbed through the intraparticle diffusion into micropores and the interior surfaces of biochar.

Pseudo-first-order (Lagergren, 1898), Pseudo-second-order (Blanchard et al., 1984), and Elovich (Low, 1960) models were used to simulate the sorption kinetics of Cu(II), Cd(II) and Pb(II) onto BB and CB biochars:

First order $q_{t} = q_e(1- e^{-k_1 t})$ (1)

Second order $q_t = \frac{k_2 q_e^2 t}{1+k_2 q_e t}$ (2)

Elovich $q_t = \frac{1}{\beta}\ln(\beta\alpha t + 1)$ (3)

Where $qt$ (mg $g^{-1}$) and $qe$ (mg $g^{-1}$) are the amounts of sorbent sorbed at time $t$ and at equilibrium, respectively; $K_1$ ($h^{-1}$) and $K_2$ (mg $g^{-1}$ $h^{-1}$) are the first-order and second order apparent sorption rate constants, respectively; and $\alpha$ (mg $g^{-1}$ $h^{-1}$) and $\beta$ (mg $g^{-1}$) are the initial Elovich sorption and desorption rate constant at time $t$, respectively. The Levenberg-Marquardt algorithm was used to estimate the value of the model parameters to minimize the sum-of-the-squared differences between model-calculated and measured kinetic data.

Pseudo-second-order was the best model describing the sorption of Pb(II) and Cd(II) onto both biochars with $R^2 > 0.94$ (Table 2). This finding suggested that sorption of Pb(II) and Cd(II) onto BB and CB is mainly controlled by chemisorptions through ion exchange, surface complexation and/or precipitation. Several previous studies have illustrated that Pseudo-second-order is better for description of Pb(II) and Cd(II) sorption onto biochars as compared to Pseudo-first -order and

Elovich models (Abdelhafez and Li, 2016; Ding et al., 2016a; Kołodyńska et al., 2012). However, Elovich model fitted the data of Cu(II) sorption better than other models ($R^2$ > 0.95 for both biochars), which support the participation of chemisorptions on the heterogeneous surfaces through the complexation by active functional groups or exchanging with sorbed cations (Jin et al., 2016). Sorption capacities of heavy metal ions onto biochars calculated by Pseudo-second-order model followed the order: Pb(II) (241.94 and 100.69 mg $g^{-1}$) > Cd(II) (103.22 and 70.83 mg $g^{-1}$) > Cu(II) (75.59 and 56.25 mg $g^{-1}$) for BB and CB, respectively.

**3.4. Sorption isotherms.**

As cleared in Fig. 4, the extent of metal ions sorption onto biochars increased rapidly as the initial concentration increased in the sorbate solution. Thereafter, this initial rapid sorption phase became slow until sorption reached equilibrium phase. The rapid sorption rate at the low sorbate solutions is occurred due to the sufficient sorption sites on biochar surfaces. As the initial concentration of metal ions increased, sorption sites are occupied till reaching saturation of all sorption sites (equilibrium). The following isotherm models were used to describe sorption of Cu(II), Cd(II) and Pb(II) onto biochars:

Langmuir (Langmuir, 1918) $$S = \frac{S_{max}KC}{1+KC} \quad (4)$$

Freudlich (Freundlich, 1906) $$S = K_f C^n \quad (5)$$

Redlich-Peterson (Redlich & Peterson, 1959) $$S = \frac{S_{max}KC}{1+KC^r} \quad (6)$$

where $S_{max}$ (mg $g^{-1}$) is the maximum sorption capacity; $K$ (L $g^{-1}$) is the Langmuir and Redlich-Peterson adsorption constant related to the interaction bonding energies and $K_f$ ($g^{(1-n)}$ Ln $kg^{-1}$) is Freundlich equilibrium constant; $C$ (g $L^{-1}$) is the equilibrium solution concentration of the sorbate; and $n$ & $r$ are the Freundlich and Redlich-Peterson linearity constants, respectively. .

The Levenberg-Marquardt algorithm was used to estimate the value of the model parameters to minimize the sum-of-the-squared differences between model-calculated and measured isotherm data.

Sorption of Cu(II) onto BB fitted better with Langmuir and Redlich-Peterson models ($R^2$=96%) as compared with Freudlich model **(79%)** (Table **2**). For CB, Cu(II) sorption best fitted with Redlich-Peterson model ($R^2$=**97%)** as compared with Freudlich (94%) and Langmuir (90%). Sorption of Cd(II) onto CB followed Langmuir model with correlation coefficient = **97%.** Meanwhile, this correlation coefficient value was relatively low (<78%) with all models describing Cd(II) sorption onto BB. Pb(II) sorption onto BB fitted better with Freudlich and Redlich-Peterson models ($R^2$=90%) than Langmuir model ($R^2$=85%). In this regard, sorption of Pb(II) onto CB fitted better with Redlich-Peterson ($R^2$=96%) as compared with Langmuir (92%) and Freudlich (91%) models.

Redlich-Peterson isotherm describes the fitting of Langmuir and Freundlich isotherm in a combined model. It has one more fitting parameter than the Langmuir and Freundlich isotherms, which may lead to better fitting (higher $R^2$); however, the good fit of the Redlich-Peterson isotherm can provide insight about the sorption process. The linearity constant "*r*" of Redlich-Peterson lies between 0-1. Sorption process is better fitted with Freundlich model when the exponent *r* is close to zero, which implies monolayer adsorption. When this constant is close to 1.0, this means that data fitted with Langmuir isotherm model. In general, the obtained values of "*r*" constant were almost close to 1.0, which indicate better fitting with Langmuir isotherm model. The Langmuir maximum sorption capacity values ($S_{max}$) of BB was much greater than those of CB. Sorption capacity of both BB and CB was higher than many feedstock reported in literature (Table 3). Overall, sorption capacity followed the order: Pb(II) (247.10 *vs.* 177.82 mg

$g^{-1}$) > Cd(II) (121.31 *vs.*73.80 mg $g^{-1}$) > Cu(II) (75.99 *vs.* 53.96 mg $g^{-1}$) for BB and CB, respectively.

**3.4. Sorption mechanisms.**

The rapid initial phase pronounced by the kinetic modeling of sorption data confirmed the participation of physisorption mechanism in metal ions sorption onto biochar. This mechanism is mainly governed by Van der Waals forces existed between sorbent and sorbate. Due to its higher electronegativity, this initial sorption phase appeared faster in BB as compared with CB.

For understanding chemisorptions mechanisms responsible for Cu(II), Pb(II) and Cd(II) sorption onto BB and CB biochars, the post-sorption samples were subjected to nanosphere morphologies SEM/EDS and XRD spectra analysis. Heavy metal deposits were clearly observed on BB and CB nanospheres, which appeared in the tubular structures formation inside the complicated network of micro-pores and cracks (Fig. 1B and 1D). The formation of heavy metal deposits was further confirmed by EDS analysis. The EDS analysis of post-sorption samples showed lowering or disappearance of the high K-peak existed in the pristine biochar with appearance of other elevated Pb(II), Cu(II) and Cd(II) peaks (Figs. 1b and d). These findings suggested the contribution of ion exchange (particularly with sorbed $K^+$ ions), precipitation, outer-and inner-sphere complexation mechanisms in the sorption of Cu(II), Pb(II) and Cd(II) ions. Potassium is easily exchanged with other metal ions since it is not involved in the organic compounds of feedstock (Marschner, 1995).

To understand mechanisms of precipitation force for sorption of Cu(II), Pb(II) and Cd(II) ions, XRD analyses were carried out on mono-element sorption and multi-element sorption experiments (Fig. 2). The XRD spectra of the mono-element sorption experiments showed the formation of precipitated minerals, which were not existed in the pristine biohar. XRD spectra of

Pb-loaded biochar samples revealed the formation of Cerussite ($PbCO_3$) on BB and Hydrocerussite ($Pb_3(CO_3)_2(OH)_2$) on CB. The deposits of Cd-crystals were existed in Otavite ($CdCO_3$) minerals formation in both biochars. Cu-loaded biochar showed elevated weak peaks of Cu-mineral in the form of Cuprite ($Cu_2O$) with BB and Posnjakite ($Cu_4(OH)_6SO_4.H_2O$) with CB. This obvious difference in precipitation form could be attributed to the high S content of CB, which favored Posnjakite formation. These findings confirmed the participation of precipitation mechanism in the sorption of Cu(II), Pb(II) and Cd(II) ions onto BB and CB.

Zeta potential (ζ) values are used to describe the electrostatic potential of the sorbent material. The density of this charge attracts the oppositely charged ions (counter ions) and driving away the like-charged ions (co-ions). As mentioned earlier, ζ analysis revealed the high electronegativity of biochars (-93.77 and -36 mV for BB and CB, respectively). This is mainly revealed to the high K content in the original feedstock, and the dominance of K-ions onto BB and CB surfaces. The valency and size of the counter ion affect ζ value and the surface adhesion equilibrium through changing the thickness of the electrical double layer and the exact location of the outer Helmholtz plane (Kirby and Hasselbrink, 2004). In this regards, there are several reports cleared a reduction in zeta potential with high valency ions (e.g. $Al^{+3}$, $Ca^{2+}$ and $Mg^{2+}$) as compared with monovalent ions (e.g. $Na^{+}$ and $K^{+}$) (Kara et al., 2008; SAKA and GÜLER, 2006). Although CB exhibited higher surface area and a complicated network of micro-pores and cracks, the higher sorption capacity of BB suggested that electrostatic attraction is the dominant force for metal ions sorption onto biochar based on its higher electronegativity.

**3.5. Effect of pH**

The pH value of the sorbate solution is one of the main factors affecting sorption process. Sorption of Cu(II), Cd(II) and Pb(II) ions onto biochars increased with the increase of pH value

of the sorbate solution (Fig. 5). This trend, however, was not the same with Pb(II) sorption onto CB as a slight reduction occurred in sorption capacity with increasing pH from 5.0 to 6.0. More than 95% of the sorbed Cu(II) onto BB and CB were accomplished at pH 4.0. This sorption capacity increased to reach about 99% at pH 6.0 (73.66 and 78.6 mg $g^{-1}$ with BB and CB, respectively). Sorption capacity of Cd(II) ions onto BB and CB was also greater at high pH values (8.0) with 74.14 and 73.20 mg $g^{-1}$, respectively. Sorption of Pb(II) onto biochars exhibited the same trend of Cu(II) sorption with about 95% sorption capacity at pH 4.0, and about 99% at pH 6.0. Unlike BB, CB showed a slight reduction in Pb(II) sorption with increasing pH value from 5.0 (72.76 mg $g^{-1}$) to 6.0 (72.74 mg $g^{-1}$). Numerous studies mentioned about the reduction of sorption capacity at lower pH values (Ding et al., 2016a; Wang et al., 2016; Xu and Zhao, 2013). This pH-dependent sorption is mainly associated with protonation or hydroxylation of the pH-dependent charges. The electrostatic repulsion between Cu(II), Cd(II) and Pb(II) ions and the predominantly positively charged colloidal surfaces, and the other competition between the abundance $H^+$ ions and those metal ions might reduce their sorption capacity onto sorbent materials at low pH values (<5.0) (Luo et al., 2017; Ma et al., 2016; Peng et al., 2016). With increasing the pH of the sorbate solution, deprotonation of different functional groups existed on biochar surfaces might provide more negatively charged sites, which favored coordination with positively charged metal ions (Ding et al., 2016a; Kołodyńska et al., 2012; Li et al., 2016). For example, at pH values ranged between 5.0 - 0.6, Cd is existed in the form $Cd(OH)^+$. This might cause an increment in its sorption onto biochars (Li et al., 2016). Another mechanism for sorption of Cd(II) ions might arise with increasing the pH value (> 6.0) through precipitation in hydroxide forms (Inyang et al., 2011; Wang et al., 2015).

The rich-K content of both biochars, which existed in several K-minerals, led to increase the final pH value of the sorbate solution although the initial pH value was readjusted twice to acidic values. This is mainly attributed to the buffering capacity of both biochars presented in its K-minerals and active functional groups. In this regard, BB showed high buffering capacity as compared with CB. Presumably, due to the presence of K in phosphate (monetite, $CaHPO_4$) and bicarbonate (kalicinite, $KHCO_3$) forms in addition to the chloride form (sylvite, KCl). However, K existed mainly as sylvite in CB. Sylvite is highly soluble mineral, which could be easily leached during sorption process. This might result in minimizing the buffering action of K-minerals. Furthermore, the precipitation of metal ions in carbonate or phosphate complexes onto BB might cause a progressive increase in the pH value of the sorbate solution (Kołodyńska et al. (2012).

**3.5. Effect of competitive sorption**

Metal ions of Cu(II), Cd(II) and Pb(II), each having the concentration of 0.2 mM, were further subjected to multi-element sorption studies onto BB and CB (0.5:200 w:v). As previously found in kinetic and isotherm experiments, sorption capacity of BB was considerably higher than CB (Fig. 6). Sorption dynamics of heavy metal ions showed a competitive sorption following this order: Pb(II) > Cu(II) > Cd(II). The removal efficiency of Pb(II) by BB reached about 98.2%, which was greater than those of Cu(II) (46.4%) and Cd(II) (7.4%). However, these removal efficiencies by CB recorded 74.6, 34.2 and 6.4% for Pb(II) > Cu(II) > Cd(II), respectively. This finding was in harmony with previous studies on biochar derived from canola and peanut straw (Xu and Zhao, 2013), water hyacinths ((Ding et al., 2016a) and rice husk and dairy manure (Xu et al., 2013a). This finding was supported by EDS spectra, which showed a high peaks of Pb(II) and Cu(II) with a very low Cd peak with BB. This low Cd(II) peak was not existed on CB.

Further to this, XRD pattern confirmed this result, which appeared through the presence of participated Cerussite ($PbCO_3$) on BB and Sussanite ($Pb_4SO_4[CO_3]_2(OH)_2$) on CB. Competitive sorption of metal ions onto sorbent materials is influenced by a number of factors, e.g. hydrolysis constant, radii of the hydrated ions, metal electronegativity, and the charge they carry (Shi et al., 2009). Having the same valency, sorption of these metal ions might be governed by their electronegativity and atomic radii. The electronegativity of Cu(II), Cd(II) and Pb(II) is 1.90, 0.69, 2.33, respectively. Accordingly, Pb(II) ions with higher electronegativity (2.33) might have sorption preferentially than Cu(II) (1.90) and Cd(II) (0.69). Beside the higher electronegativity, the higher atomic radii, thereby the lower hydrated radii might maximize the competitive sorption of Pb(II) (ionic radius = 122 pm; hydrated radius = 261 pm) and Cu(II) (ionic radius = 72 pm; hydrated radius = 295 pm).

**4. Conclusion**

Chemical activation of biochar is widely used for increasing its sorption capacity to be able to compensate other conventional adsorbents. Several drawbacks, however, arise surrounding the excessive use of chemicals during impregnation, neutralization and drying of the activated biochar including the extra laborious activation work and the generation of huge amounts of hazardous chemical sludge. To overcome these economic and environmental drawbacks, this work is highlighting the potential in-situ activation of biochar during pyrolysis through the inherent K-compounds of the organic feedstock (banana peels and cauliflower leaves). The inherent rich-K content exhibited a catalytic effect during pyrolysis, and generated biochars (BB and CB) with high electronegativity. BB showed higher sorption capacity although CB recorded higher surface area (<5.0 *vs.* 12.5 $m^2$ $g^{-1}$). Electrostatic attraction was the dominant mechanism

controlling sorption process with partial contributions of physisorption, ion exchange and precipitation. This was confirmed by the higher sorption capacity of BB, which possess higher ζ value comparing with CB (-93.77 *vs.* -36.42 mv). Sorption of metal ions onto biochars was pH-dependent, and showed the order: Pb(II) > Cu(II) > Cd(II). Further investigations are needed to explore the effect of pyrolysis temperature on productivity and sorption capacity of biochar derived from K-rich feedstock.

**Acknowledgments**

This research was partially supported by the NSF through Grant CBET-1054405 and the Fulbright Program of United State of America (USEF-Pakistan). Authors are also grateful to Dr. Willie G. Harris, Soil and Water Science Department, University of Florida, Gainesville, FL for his valuable suggestions in interpretation of XRD data.

**Figure Caption:**

Figure 1: Scanning electron microscope (SEM) (A, B, C, D) and respective energy dispersive X-ray spectrometry (EDS) (a, b, c, d) results of BB and CB.

Figure 2. XRD analysis BB and CB impregnated with Cu(II), Cd(II) and Pb(II) in single and binary system.

Figure 3. Kinatics of Cu(II), Cd(II) and Pb(II) adsroption on BB and CB.

Figure 4. Isotherm of Cu(II), Cd(II) and Pb(II) adsorption on BB and CB.

Figure 5. Effect of pH of initial solution on adsorption of Cu(II), Cd(II) and Pb(II) by BB and CB.

Figure 6. Removal (%) of Cu(II), Cd(II) and Pb(II) from mixed solution by BB and CB.

**Table Caption:**

Table 1: Selected physico-chemical properties of biochars used in current study.

Table 2: Kinetics and isotherm models and best-fit parameters for Cu(II), Cd(II) and Pb(II) sorption onto BB and CB.

Table 3: Comparison of BB and CB adsorption capacity of Cu(II), Cd(II) and Pb(II) with other biosorbents.

Comment: this table is here just to keep the references in "Reference list"

Table 3. Comparison of BB and CB adsorption capacity of Cu(II), Cd(II) and Pb(II) with other biosorbents.

| **Metal** | **Biosorbents** | **Sorption capacity (mg $g^{-1}$)** | **Reference** |
|---|---|---|---|
| Cu | Banan peels biochar | 75.99 | Current study |
| | Cauliflower leaves biochar | 53.96 | Current study |
| | Commercial powdered activated carbon (PAC) | 1.32 | (Liu et al., 2014) |
| | Humic acid treated PAC | 5.95 | (Liu et al., 2014) |
| | Green vegetable waste derived activated carbon | 75 | (Sabela et al., 2016) |
| | Dairy manure biochar | 54.4 | (Xu et al., 2013b) |
| | Grape stalk waste | 15.9 | (Villaescusa et al., 2004) |
| | *Tamarindus indica* seed powder | 82.97 | (Chowdhury and Saha, 2011) |
| | *Cinnamomum camphora* leaves powder | 16.75 | (Chen et al., 2010) |
| | Rose waste biomass | 55.79 | (Iftikhar et al., 2009) |
| | Sour orange residue | 21.7 | (Khormaei et al., 2007) |
| | Thermal power plants ash | 5.75 | (Tofan et al., 2008) |
| | Carrot residue | 32.7 | (Nasernejad et al., 2005) |
| | Root of rose biochar | 60.7 | (Khare et al., 2013) |
| Cd | Banan peels biochar | 121.3 | Current study |
| | Cauliflower leaves biochar | 73.8 | Current study |
| | Commercial activated carbon | 8 | (Mohan et al., 2007) |
| | Apricot stone activated carbon | 33.57 | (Kobya et al., 2005) |
| | Dairy manure biochar | 51.4 | (Xu et al., 2013b) |
| | Bagasse fly ash | 1.24 | (Gupta et al., 2003) |

| | | | |
|---|---|---|---|
| | Root of rose biochar | 66.36 | (Khare et al., 2013) |
| | Pine bark biochar | 0.34 | (Mohan et al., 2007) |
| | Water hyacinth biochar | 77.5 | (Ding et al., 2016a) |
| Pb | Banan peels biochar | 247.1 | Current study |
| | Cauliflower leaves biochar | 177.8 | Current study |
| | Root of rose biochar | 52.95 | (Khare et al., 2013) |
| | Pine bark biochar | 3.0 | (Mohan et al., 2007) |
| | Commercial activated carbon | 30.11 | (Mohan et al., 2007) |
| | Water hyacinth biochar | 168 | (Ding et al., 2016a) |
| | Apricot stone activated carbon | 22.85 | (Kobya et al., 2005) |
| | Digested whole sugar beet biochar | 40.82 | (Inyang et al., 2011) |
| | Digested dairy waste biochar | 51.38 | (Inyang et al., 2011) |

References

Abdelhafez, A.A., Li, J., 2016. Removal of Pb(II) from aqueous solution by using biochars derived from sugar cane bagasse and orange peel. Journal of the Taiwan Institute of Chemical Engineers 61, 367-375.
Al-Shannag, M., Al-Qodah, Z., Bani-Melhem, K., Qtaishat, M.R., Alkasrawi, M., 2015. Heavy metal ions removal from metal plating wastewater using electrocoagulation: Kinetic study and process performance. Chemical Engineering Journal 260, 749-756.
Ali, M.M., Ali, M.L., Islam, M.S., Rahman, M.Z., 2016. Preliminary assessment of heavy metals in water and sediment of Karnaphuli River, Bangladesh. Environmental Nanotechnology, Monitoring & Management 5, 27-35.
Blanchard, G., Maunaye, M., Martin, G., 1984. Removal of heavy metals from waters bymeans of natural zeolites. Water Research 18, 1501-1507.
Branca, C., Di Blasi, C., 2015. A lumped kinetic model for banana peel combustion. Thermochimica Acta 614, 68-75.
Chen, H., Dai, G., Zhao, J., Zhong, A., Wu, J., Yan, H., 2010. Removal of copper(II) ions by a biosorbent—Cinnamomum camphora leaves powder. Journal of Hazardous Materials 177, 228-236.
Chen, J., Li, S., Liang, C., Xu, Q., Li, Y., Qin, H., Fuhrmann, J.J., 2017. Response of microbial community structure and function to short-term biochar amendment in an intensively managed bamboo (Phyllostachys praecox) plantation soil: Effect of particle size and addition rate. Science of The Total Environment 574, 24-33.
Chen, M., Qin, X., Zeng, G., Li, J., 2016. Impacts of human activity modes and climate on heavy metal “spread” in groundwater are biased. Chemosphere 152, 439-445.
Chen, Y.-D., Huang, M.-J., Huang, B., Chen, X.-R., 2012. Mesoporous activated carbon from inherently potassium-rich pokeweed by in situ self-activation and its use for phenol removal. Journal of Analytical and Applied Pyrolysis 98, 159-165.
Chowdhury, P., Athapaththu, S., Elkamel, A., Ray, A.K., 2017. Visible-solar-light-driven photo-reduction and removal of cadmium ion with Eosin Y-sensitized TiO2 in aqueous solution of triethanolamine. Separation and Purification Technology 174, 109-115.
Chowdhury, S., Saha, P.D., 2011. Biosorption kinetics, thermodynamics and isosteric heat of sorption of Cu(II) onto Tamarindus indica seed powder. Colloids and Surfaces B: Biointerfaces 88, 697-705.
Creamer, A.E., Gao, B., Wang, S., 2016. Carbon dioxide capture using various metal oxyhydroxide–biochar composites. Chemical Engineering Journal 283, 826-832.
Creamer, A.E., Gao, B., Zhang, M., 2014. Carbon dioxide capture using biochar produced from sugarcane bagasse and hickory wood. Chemical Engineering Journal 249, 174-179.
Dehkhoda, A.M., Gyenge, E., Ellis, N., 2016. A novel method to tailor the porous structure of KOH-activated biochar and its application in capacitive deionization and energy storage. Biomass and Bioenergy 87, 107-121.
Ding, W., Dong, X., Ime, I.M., Gao, B., Ma, L.Q., 2014. Pyrolytic temperatures impact lead sorption mechanisms by bagasse biochars. Chemosphere 105, 68-74.
Ding, Y., Liu, Y., Liu, S., Li, Z., Tan, X., Huang, X., Zeng, G., Zhou, Y., Zheng, B., Cai, X., 2016a. Competitive removal of Cd (II) and Pb (II) by biochars produced from water hyacinths: performance and mechanism. RSC Advances 6, 5223-5232.

Ding, Z., Wan, Y., Hu, X., Wang, S., Zimmerman, A.R., Gao, B., 2016b. Sorption of lead and methylene blue onto hickory biochars from different pyrolysis temperatures: Importance of physicochemical properties. Journal of Industrial and Engineering Chemistry 37, 261-267.
Edebali, S., Pehlivan, E., 2016. Evaluation of chelate and cation exchange resins to remove copper ions. Powder Technology 301, 520-525.
Enders, A., Lehmann, J., 2012. Comparison of Wet-Digestion and Dry-Ashing Methods for Total Elemental Analysis of Biochar. Communications in Soil Science and Plant Analysis 43, 1042-1052.
Freundlich, H.M.F., 1906. Uber die adsorption in lasungen. Journal of Physical Chemistry 57, 385–370.
Fu, F., Xie, L., Tang, B., Wang, Q., Jiang, S., 2012. Application of a novel strategy—Advanced Fenton-chemical precipitation to the treatment of strong stability chelated heavy metal containing wastewater. Chemical Engineering Journal 189–190, 283-287.
Gao, X., Zhou, F., Chen, C.-T.A., Xing, Q., 2015. Trace metals in the suspended particulate matter of the Yellow River (Huanghe) Estuary: Concentrations, potential mobility, contamination assessment and the fluxes into the Bohai Sea. Continental Shelf Research 104, 25-36.
Gupta, V.K., Jain, C.K., Ali, I., Sharma, M., Saini, V.K., 2003. Removal of cadmium and nickel from wastewater using bagasse fly ash—a sugar industry waste. Water Research 37, 4038-4044.
Hao, Q.-l., Li, B.-l., Lei, L.I.U., Zhang, Z.-b., Dou, B.-j., Chang, W., 2015. Effect of potassium on pyrolysis of rice husk and its components. Journal of Fuel Chemistry and Technology 43, 34-41.
Hebbar, R.S., Isloor, A.M., Ananda, K., Ismail, A.F., 2016. Fabrication of polydopamine functionalized halloysite nanotube/polyetherimide membranes for heavy metal removal. Journal of Materials Chemistry A 4, 764-774.
Hua, M., Zhang, S., Pan, B., Zhang, W., Lv, L., Zhang, Q., 2012. Heavy metal removal from water/wastewater by nanosized metal oxides: A review. Journal of Hazardous Materials 211–212, 317-331.
Huynh, N.T., Smagghe, G., Gonzales, G.B., Van Camp, J., Raes, K., 2016. Extraction and bioconversion of kaempferol metabolites from cauliflower outer leaves through fungal fermentation. Biochemical Engineering Journal 116, 27-33.
Iftikhar, A.R., Bhatti, H.N., Hanif, M.A., Nadeem, R., 2009. Kinetic and thermodynamic aspects of Cu(II) and Cr(III) removal from aqueous solutions using rose waste biomass. Journal of Hazardous Materials 161, 941-947.
Inyang, M., Gao, B., Ding, W., Pullammanappallil, P., Zimmerman, A.R., Cao, X., 2011. Enhanced Lead Sorption by Biochar Derived from Anaerobically Digested Sugarcane Bagasse. Separation Science and Technology 46, 1950-1956.
Inyang, M., Gao, B., Zimmerman, A., Zhang, M., Chen, H., 2014. Synthesis, characterization, and dye sorption ability of carbon nanotube–biochar nanocomposites. Chemical Engineering Journal 236, 39-46.
Inyang, M., Gao, B., Pullammanappallil, P., Ding, W., Zimmerman, A.R., 2010. Biochar from anaerobically digested sugarcane bagasse. Bioresource Technology 101, 8868-8872.
Inyang, M., Gao, B., Yao, Y., Xue, Y., Zimmerman, A.R., Pullammanappallil, P., Cao, X., 2012. Removal of heavy metals from aqueous solution by biochars derived from anaerobically digested biomass. Bioresource Technology 110, 50-56.

Inyang, M.I., Gao, B., Yao, Y., Xue, Y., Zimmerman, A., Mosa, A., Pullammanappallil, P., Ok, Y.S., Cao, X., 2016. A review of biochar as a low-cost adsorbent for aqueous heavy metal removal. Critical Reviews in Environmental Science and Technology 46, 406-433.
Jin, H., Hanif, M.U., Capareda, S., Chang, Z., Huang, H., Ai, Y., 2016. Copper (II) removal potential from aqueous solution by pyrolysis biochar derived from anaerobically digested algae-dairy-manure and effect of KOH activation. Journal of Environmental Chemical Engineering 4, 365-372.
Johnson, P.R., Sun, N., Elimelech, M., 1996. Colloid transport in geochemically heterogeneous porous media: Modeling and measurements. Environmental science & technology 30, 3284-3293.
Kara, F., Gurakan, G.C., Sanin, F.D., 2008. Monovalent cations and their influence on activated sludge floc chemistry, structure, and physical characteristics. Biotechnology and Bioengineering 100, 231-239.
Khare, P., Dilshad, U., Rout, P.K., Yadav, V., Jain, S., 2013. Plant refuses driven biochar: Application as metal adsorbent from acidic solutions. Arabian Journal of Chemistry.
Khormaei, M., Nasernejad, B., Edrisi, M., Eslamzadeh, T., 2007. Copper biosorption from aqueous solutions by sour orange residue. Journal of Hazardous Materials 149, 269-274.
Kirby, B.J., Hasselbrink, E.F., 2004. Zeta potential of microfluidic substrates: 1. Theory, experimental techniques, and effects on separations. ELECTROPHORESIS 25, 187-202.
Kobya, M., Demirbas, E., Senturk, E., Ince, M., 2005. Adsorption of heavy metal ions from aqueous solutions by activated carbon prepared from apricot stone. Bioresource Technology 96, 1518-1521.
Kołodyńska, D., Wnętrzak, R., Leahy, J.J., Hayes, M.H.B., Kwapiński, W., Hubicki, Z., 2012. Kinetic and adsorptive characterization of biochar in metal ions removal. Chemical Engineering Journal 197, 295-305.
Lagergren, S., 1898. Zur theorie der sogenannten adsorption gelöster stoffe, Kungliga Svenska Vetenskapsakademiens. Handlingar 24, 1-39.
Langmuir, I., 1918. The adsorption of gases on plane surfaces of glass, mica and platinum. American Chemical Society 40, 1361-1403.
Lehmann, J., 2007. Bio□energy in the black. Frontiers in Ecology and the Environment 5, 381-387.
Li, F., Shen, K., Long, X., Wen, J., Xie, X., Zeng, X., Liang, Y., Wei, Y., Lin, Z., Huang, W., Zhong, R., 2016. Preparation and Characterization of Biochars from <italic>Eichornia crassipes</italic> for Cadmium Removal in Aqueous Solutions. PLoS ONE 11, e0148132.
Li, J., Chen, C., Zhang, R., Wang, X., 2015. Nanoscale Zero-Valent Iron Particles Supported on Reduced Graphene Oxides by Using a Plasma Technique and Their Application for Removal of Heavy-Metal Ions. Chemistry – An Asian Journal 10, 1410-1417.
Liu, H., Feng, S., Zhang, N., Du, X., Liu, Y., 2014. Removal of Cu(II) ions from aqueous solution by activated carbon impregnated with humic acid. Frontiers of Environmental Science & Engineering 8, 329-336.
Low, M.J.D., 1960. Kinetics of Chemisorption of Gases on Solids. Chemical Reviews 60, 267-312.
Luo, X., Yu, L., Wang, C., Yin, X., Mosa, A., Lv, J., Sun, H., 2017. Sorption of vanadium (V) onto natural soil colloids under various solution pH and ionic strength conditions. Chemosphere 169, 609-617.

Ma, J., Guo, H., Lei, M., Wan, X., Zhang, H., Feng, X., Wei, R., Tian, L., Han, X., 2016. Blocking effect of colloids on arsenate adsorption during co-transport through saturated sand columns. Environmental Pollution 213, 638-647.
Marschner, H., 1995. Mineral Nutrition of Higher Plants. Academic Press.
Mohan, D., Pittman Jr, C.U., Bricka, M., Smith, F., Yancey, B., Mohammad, J., Steele, P.H., Alexandre-Franco, M.F., Gómez-Serrano, V., Gong, H., 2007. Sorption of arsenic, cadmium, and lead by chars produced from fast pyrolysis of wood and bark during bio-oil production. Journal of Colloid and Interface Science 310, 57-73.
Mosa, A., El-Banna, M.F., Gao, B., 2016. Biochar filters reduced the toxic effects of nickel on tomato (Lycopersicon esculentum L.) grown in nutrient film technique hydroponic system. Chemosphere 149, 254-262.
Mosa, A.A., El-Ghamry, A., Trüby, P., 2011. Chemically Modified Crop Residues as a Low-Cost Technique for the Removal of Heavy Metal Ions from Wastewater. Water, Air, & Soil Pollution 217, 637-647.
Nasernejad, B., Zadeh, T.E., Pour, B.B., Bygi, M.E., Zamani, A., 2005. Camparison for biosorption modeling of heavy metals (Cr (III), Cu (II), Zn (II)) adsorption from wastewater by carrot residues. Process Biochemistry 40, 1319-1322.
Nouri, J., Mahvi, A.H., Jahed, G.R., Babaei, A.A., 2008. Regional distribution pattern of groundwater heavy metals resulting from agricultural activities. Environmental Geology 55, 1337-1343.
Nowakowski, D.J., Jones, J.M., 2008. Uncatalysed and potassium-catalysed pyrolysis of the cell-wall constituents of biomass and their model compounds. Journal of Analytical and Applied Pyrolysis 83, 12-25.
Nowakowski, D.J., Jones, J.M., Brydson, R.M.D., Ross, A.B., 2007. Potassium catalysis in the pyrolysis behaviour of short rotation willow coppice. Fuel 86, 2389-2402.
Peng, P., Lang, Y.-H., Wang, X.-M., 2016. Adsorption behavior and mechanism of pentachlorophenol on reed biochars: pH effect, pyrolysis temperature, hydrochloric acid treatment and isotherms. Ecological Engineering 90, 225-233.
Rajapaksha, A.U., Chen, S.S., Tsang, D.C.W., Zhang, M., Vithanage, M., Mandal, S., Gao, B., Bolan, N.S., Ok, Y.S., 2016. Engineered/designer biochar for contaminant removal/immobilization from soil and water: potential and implication of biochar modification. Chemosphere 148, 6e291.
Redlich, O., Peterson, D.L., 1959. A Useful Adsorption Isotherm. The Journal of Physical Chemistry 63, 1024-1024.
Rybarczyk, M.K., Lieder, M., Jablonska, M., 2015. N-doped mesoporous carbon nanosheets obtained by pyrolysis of a chitosan-melamine mixture for the oxygen reduction reaction in alkaline media. RSC Advances 5, 44969-44977.
Sabela, M.I., Kunene, K., Kanchi, S., Xhakaza, N.M., Bathinapatla, A., Mdluli, P., Sharma, D., Bisetty, K., 2016. Removal of copper (II) from wastewater using green vegetable waste derived activated carbon: An approach to equilibrium and kinetic study. Arabian Journal of Chemistry.
SAKA, E.E., GÜLER, C., 2006. The effects of electrolyte concentration, ion species and pH on the zeta potential and electrokinetic charge density of montmorillonite. Clay Minerals 41, 853-861.
Shi, T., Jia, S., Chen, Y., Wen, Y., Du, C., Guo, H., Wang, Z., 2009. Adsorption of Pb(II), Cr(III), Cu(II), Cd(II) and Ni(II) onto a vanadium mine tailing from aqueous solution. Journal of Hazardous Materials 169, 838-846.

Stoewsand, G.S., 1995. Bioactive organosulfur phytochemicals in Brassica oleracea vegetables—A review. Food and Chemical Toxicology 33, 537-543.
Suliman, W., Harsh, J.B., Abu-Lail, N.I., Fortuna, A.-M., Dallmeyer, I., Garcia-Pérez, M., 2017. The role of biochar porosity and surface functionality in augmenting hydrologic properties of a sandy soil. Science of The Total Environment 574, 139-147.
Sun, Y., Gao, B., Yao, Y., Fang, J., Zhang, M., Zhou, Y., Chen, H., Yang, L., 2014. Effects of feedstock type, production method, and pyrolysis temperature on biochar and hydrochar properties. Chemical Engineering Journal 240, 574-578.
Tofan, L., Paduraru, C., Bilba, D., Rotariu, M., 2008. Thermal power plants ash as sorbent for the removal of Cu(II) and Zn(II) ions from wastewaters. Journal of Hazardous Materials 156, 1-8.
Varol, M., Şen, B., 2012. Assessment of nutrient and heavy metal contamination in surface water and sediments of the upper Tigris River, Turkey. CATENA 92, 1-10.
Villaescusa, I., Fiol, N., Martínez, M.a., Miralles, N., Poch, J., Serarols, J., 2004. Removal of copper and nickel ions from aqueous solutions by grape stalks wastes. Water Research 38, 992-1002.
Wang, H., Gao, B., Wang, S., Fang, J., Xue, Y., Yang, K., 2015. Removal of Pb(II), Cu(II), and Cd(II) from aqueous solutions by biochar derived from KMnO4 treated hickory wood. Bioresource Technology 197, 356-362.
Wang, Y.-Y., Lu, H.-H., Liu, Y.-X., Yang, S.-M., 2016. Removal of phosphate from aqueous solution by SiO2-biochar nanocomposites prepared by pyrolysis of vermiculite treated algal biomass. RSC Advances 6, 83534-83546.
Wuana, R.A., Okieimen, F.E., 2011. Heavy Metals in Contaminated Soils: A Review of Sources, Chemistry, Risks and Best Available Strategies for Remediation. ISRN Ecology 2011, 20.
Xiao, Y., Xue, Y., Gao, F., Mosa, A., 2017. Sorption of heavy metal ions onto crayfish shell biochar: Effect of pyrolysis temperature, pH and ionic strength. Journal of the Taiwan Institute of Chemical Engineers 80, 114-121.

Xu, R.-k., Zhao, A.-z., 2013. Effect of biochars on adsorption of Cu(II), Pb(II) and Cd(II) by three variable charge soils from southern China. Environmental Science and Pollution Research 20, 8491-8501.
Xu, X., Cao, X., Zhao, L., 2013a. Comparison of rice husk- and dairy manure-derived biochars for simultaneously removing heavy metals from aqueous solutions: Role of mineral components in biochars. Chemosphere 92, 955-961.
Xu, X., Cao, X., Zhao, L., Wang, H., Yu, H., Gao, B., 2013b. Removal of Cu, Zn, and Cd from aqueous solutions by the dairy manure-derived biochar. Environmental Science and Pollution Research 20, 358-368.
Xu, Y., Li, Y., Bao, T., Zheng, X., Chen, W., Wang, J., 2017. A recyclable protein resource derived from cauliflower by-products: Potential biological activities of protein hydrolysates. Food Chemistry 221, 114-122.
Xue, L., Gao, B., Wan, Y., Fang, J., Wang, S., Li, Y., Muñoz-Carpena, R., Yang, L., 2016. High efficiency and selectivity of MgFe-LDH modified wheat-straw biochar in the removal of nitrate from aqueous solutions. Journal of the Taiwan Institute of Chemical Engineers 63, 312-317.
Xue, Y., Gao, B., Yao, Y., Inyang, M., Zhang, M., Zimmerman, A.R., Ro, K.S., 2012. Hydrogen peroxide modification enhances the ability of biochar (hydrochar) produced from hydrothermal carbonization of peanut hull to remove aqueous heavy metals: Batch and column tests. Chemical Engineering Journal 200–202, 673-680.

Yao, Y., Gao, B., Chen, J., Zhang, M., Inyang, M., Li, Y., Alva, A., Yang, L., 2013. Engineered carbon (biochar) prepared by direct pyrolysis of Mg-accumulated tomato tissues: Characterization and phosphate removal potential. Bioresource Technology 138, 8-13.
Ye, M., Sun, M., Wan, J., Fang, G., Li, H., Hu, F., Jiang, X., Orori Kengara, F., 2015. Evaluation of enhanced soil washing process with tea saponin in a peanut oil–water solvent system for the extraction of PBDEs/PCBs/PAHs and heavy metals from an electronic waste site followed by vetiver grass phytoremediation. Journal of Chemical Technology & Biotechnology 90, 2027-2035.
Yu, F., Zhou, Y., Gao, B., Qiao, H., Li, Y., Wang, E., Pang, L., Bao, C., 2016. Effective removal of ionic liquid using modified biochar and its biological effects. Journal of the Taiwan Institute of Chemical Engineers 67, 318-324.
Zeraatkar, A.K., Ahmadzadeh, H., Talebi, A.F., Moheimani, N.R., McHenry, M.P., 2016. Potential use of algae for heavy metal bioremediation, a critical review. Journal of Environmental Management 181, 817-831.
Zhang, M., Gao, B., Yao, Y., Xue, Y., Inyang, M., 2012. Synthesis, characterization, and environmental implications of graphene-coated biochar. Science of The Total Environment 435–436, 567-572.

Zhang, X., Wu, J., Yang, H., Shao, J., Wang, X., Chen, Y., Zhang, S., Chen, H. 2016. Preparation of nitrogen-doped microporous modified biochar by high temperature CO2-NH3 treatment for CO2 adsorption: effects of temperature. *RSC Advances*, **6**(100), 98157-98166.

Table 1: Selected physico-chemical properties of biochars used in current study.

| Biochars | Production rate | Elemental concentration (%, dry matter based) | | | | | | | | | | | | | | pH | Surface area | Zeta Potential |
|---|---|---|---|---|---|---|---|---|---|---|---|---|---|---|---|---|---|---|
| | (%) | C | H | N | P | K | Ca | Mg | Fe | Al | Zn | Mn | Cu | Cd | Pb | | ($m^2g^{-1}$) | (mv) |
| BB | 61.44 | 51.3 | 1.62 | 1.57 | 0.47 | 10.89 | 0.59 | 0.29 | 0.01 | 0.004 | 0.003 | 0.002 | *N.D. | N.D. | 0.008 | 10.09 | <5 | -93.77 |
| CB | 64.66 | 50.2 | 1.53 | 4.14 | 1.81 | 11.04 | 6.17 | 1.16 | 0.19 | 0.006 | 0.014 | 0.007 | N.D. | N.D. | 0.0004 | 10.64 | 12.5 | -36.42 |

* Not detected (below the detection limit)

Table 2. Kinetics and isotherm models and best-fit parameters for Cu, Cd and Pb sorption onto BB and CB.

| Element | Models | BB Model parameters | | | CB Model parameters | | |
|---|---|---|---|---|---|---|---|
| | | Parameter1 | Parameter2 | $R^2$ | Parameter1 | Parameter2 | $R^2$ |
| **Kinetic models** | | | | | | | |
| Cu | First-order | $q_e$=72.91 g $kg^{-1}$ | $K_f$=2.88 $h^{-1}$ | 0.46 | $q_e$=50.93 g $kg^{-1}$ | $K_f$=0.59 $h^{-1}$ | 0.71 |
| | Second-order | $q_e$=75.59 g $kg^{-1}$ | $k_2$=0.07 kg $g^{-1}$ $h^{-1}$ | 0.80 | $q_e$=56.25 g $kg^{-1}$ | $k_2$=0.01 kg $g^{-1}$ $h^{-1}$ | 0.80 |
| | Elovich | α=1189473 mg $g^{-1}$ | β=0.20g $mg^{-1}$ | 0.96 | α=203.88 mg $g^{-1}$ | β=0.12 g $mg^{-1}$ | 0.95 |
| Cd | First-order | $q_e$=98.44 g $kg^{-1}$ | $K_f$=1.54 $h^{-1}$ | 0.88 | $q_e$=61.60 g $kg^{-1}$ | $K_f$=0.24 $h^{-1}$ | 1.00 |
| | Second-order | $q_e$=103.22 g $kg^{-1}$ | $k_2$=0.02 kg $g^{-1}$ $h^{-1}$ | 0.94 | $q_e$=70.83 g $kg^{-1}$ | $k_2$=0.00 kg $g^{-1}$ $h^{-1}$ | 0.99 |
| | Elovich | α=5250.42 mg $g^{-1}$ | β=0.09 g $mg^{-1}$ | 0.84 | α=38.39 mg $g^{-1}$ | β=0.07 g $mg^{-1}$ | 0.95 |
| Pb | First-order | $q_e$=237.53 g $kg^{-1}$ | $K_f$=3.87 $h^{-1}$ | 0.81 | $q_e$=97.98 g $kg^{-1}$ | $K_f$=5.73 $h^{-1}$ | 0.81 |
| | Second-order | $q_e$=241.49 g $kg^{-1}$ | $k_2$=0.05 kg $g^{-1}$ $h^{-1}$ | 0.99 | $q_e$=100.69 g $kg^{-1}$ | $k_2$=0.14 kg $g^{-1}$ $h^{-1}$ | 0.97 |
| | Elovich | α=1.54 × $10^{15}$ mg $g^{-1}$ | β=0.15 g $mg^{-1}$ | 0.70 | α=4.72 × $10^{10}$ mg $g^{-1}$ | β=0.26 g $mg^{-1}$ | 0.63 |
| **Isotherm models** | | | | | | | |
| Cu | Langmuir | $q_{max}$ = 75.99 mg $g^{-1}$ | K=0.96 L $g^{-1}$ | 0.96 | $q_{max}$ = 53.96 mg $g^{-1}$ | K= 1.42 L $g^{-1}$ | 0.90 |
| | Freudlich | n= 0.17 | $K_f$= 36.2 $g^{(1-n)}$ Ln $kg^{-1}$ | 0.79 | n= 0.15 | $K_f$= 29.0 $g^{(1-n)}$ Ln $kg^{-1}$ | 0.94 |
| | Redlich-Peterson | $q_{max}$ = 83.49 mg $g^{-1}$ | K=0.81 L $g^{-1}$ r= 1.02 | 0.96 | $q_{max}$ = 36.35 mg $g^{-1}$ | K=4.70 L $g^{-1}$ r= 0.90 | 0.97 |
| Cd | Langmuir | $q_{max}$ = 121.31mg $g^{-1}$ | K=1.18 L $g^{-1}$ | 0.76 | $q_{max}$ = 73.80 mg $g^{-1}$ | K= 0.38 L $g^{-1}$ | 0.97 |
| | Freudlich | n= 0.17 | $K_f$= 56.4 $g^{(1-n)}$ Ln $kg^{-1}$ | 0.76 | n= 0.19 | $K_f$= 30.4 $g^{(1-n)}$ Ln $kg^{-1}$ | 0.90 |
| | Redlich-Peterson | $q_{max}$ = 81.22 mg $g^{-1}$ | K=3.09 L $g^{-1}$ r= 0.91 | 0.78 | $q_{max}$ = 30.40 mg $g^{-1}$ | K=8710 L $g^{-1}$ r= 0.81 | 0.90 |
| Pb | Langmuir | $q_{max}$ = 247.10 mg $g^{-1}$ | K= 2.48L $g^{-1}$ | 0.85 | $q_{max}$ = 177.82 mg $g^{-1}$ | K=1.82 L $g^{-1}$ | 0.92 |
| | Freudlich | n= 0.15 | $K_f$= 120.1 $g^{(1-n)}$ Ln $kg^{-1}$ | 0.90 | n= 0.14 | $K_f$= 91.1 $g^{(1-n)}$ Ln $kg^{-1}$ | 0.91 |
| | Redlich-Peterson | $q_{max}$ = 120.00 mg $g^{-1}$ | K=8710L $g^{-1}$ r= 0.85 | 0.90 | $q_{max}$ = 118.80 mg $g^{-1}$ | K=8.61 L $g^{-1}$ r= 0.92 | 0.96 |

Table 3. Comparison of BB and CB adsorption capacity of Cu(II), Cd(II) and Pb(II) with other biosorbents.

| **Metal** | **Biosorbents** | **Sorption capacity (mg $g^{-1}$)** | **Reference** |
|---|---|---|---|
| Cu | Banan peels biochar | 75.99 | Current study |
| | Cauliflower leaves biochar | 53.96 | Current study |
| | Commercial powdered activated carbon (PAC) | 1.32 | (Liu et al., 2014) |
| | Humic acid treated PAC | 5.95 | (Liu et al., 2014) |
| | Green vegetable waste derived activated carbon | 75 | (Sabela et al., 2016) |
| | Dairy manure biochar | 54.4 | (Xu et al., 2013b) |
| | Grape stalk waste | 15.9 | (Villaescusa et al., 2004) |
| | *Tamarindus indica* seed powder | 82.97 | (Chowdhury and Saha, 2011) |
| | *Cinnamomum camphora* leaves powder | 16.75 | (Chen et al., 2010) |
| | Rose waste biomass | 55.79 | (Iftikhar et al., 2009) |
| | Sour orange residue | 21.7 | (Khormaei et al., 2007) |
| | Thermal power plants ash | 5.75 | (Tofan et al., 2008) |
| | Carrot residue | 32.7 | (Nasernejad et al., 2005) |
| | Root of rose biochar | 60.7 | (Khare et al., 2013) |
| Cd | Banan peels biochar | 121.3 | Current study |
| | Cauliflower leaves biochar | 73.8 | Current study |
| | Commercial activated carbon | 8 | (Mohan et al., 2007) |
| | Apricot atone activated carbon | 33.57 | (Kobya et al., 2005) |
| | Dairy manure biochar | 51.4 | (Xu et al., 2013b) |
| | Bagasse fly ash | 1.24 | (Gupta et al., 2003) |
| | Root of rose biochar | 66.36 | (Khare et al., 2013) |

| | | | |
|---|---|---|---|
| | Pine bark biochar | 0.34 | (Mohan et al., 2007) |
| | Water hyacinth biochar | 77.5 | (Ding et al., 2016b) |
| Pb | Banan peels biochar | 247.1 | Current study |
| | Cauliflower leaves biochar | 177.8 | Current study |
| | Root of rose biochar | 52.95 | (Khare et al., 2013) |
| | Pine bark biochar | 3.0 | (Mohan et al., 2007) |
| | Commercial activated carbon | 30.11 | (Mohan et al., 2007) |
| | Water hyacinth biochar | 168 | (Ding et al., 2016b) |
| | Apricot atone activated carbon | 22.85 | (Kobya et al., 2005) |
| | Digested whole sugar beet biochar | 40.82 | (Inyang et al., 2011) |
| | Digested dairy waste biochar | 51.38 | (Inyang et al., 2011) |

**Figure 1.**

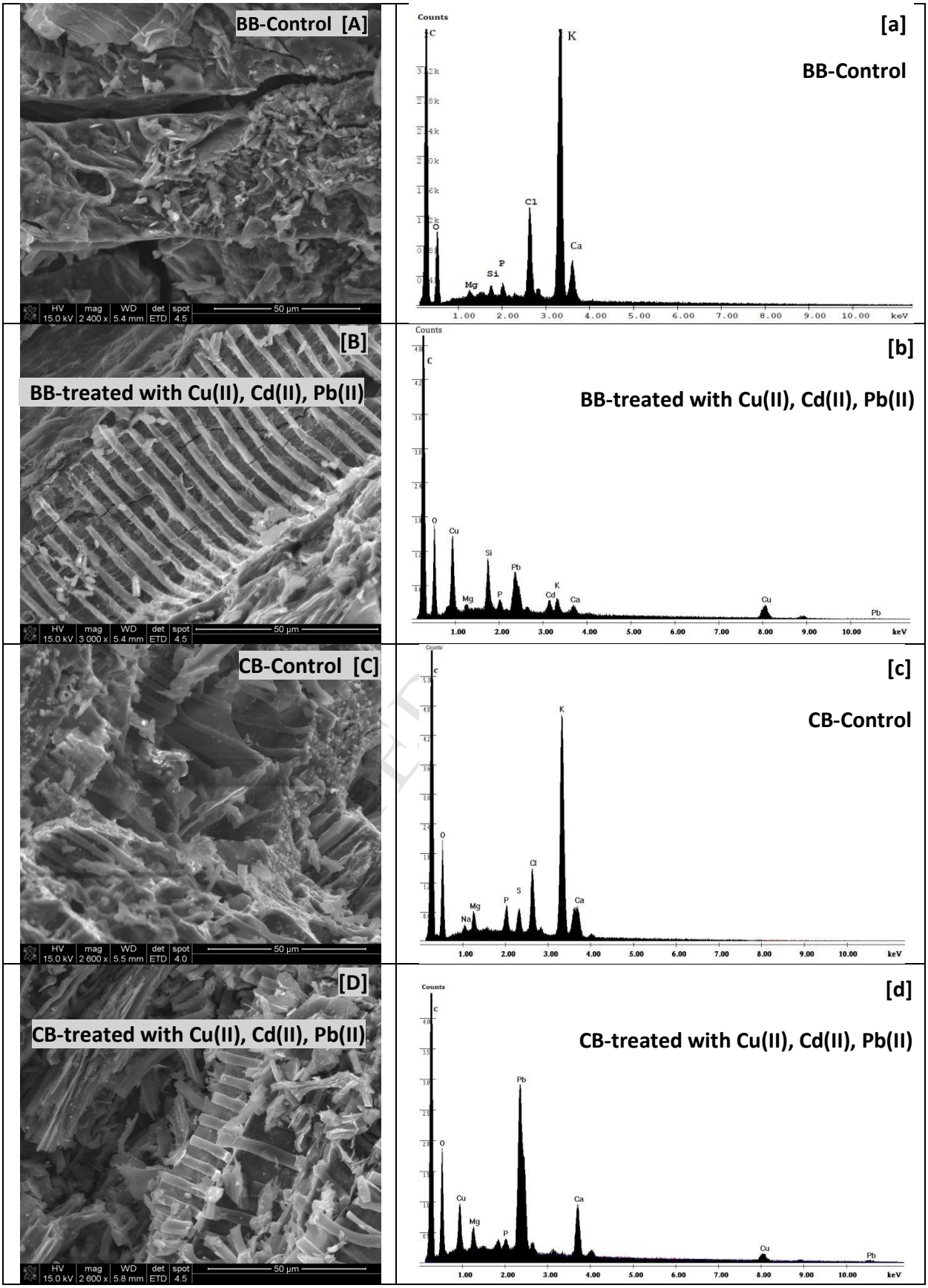
BB-Control [A]
[a]
BB-Control
[B]
BB-treated with Cu(II), Cd(II), Pb(II)
[b]
BB-treated with Cu(II), Cd(II), Pb(II)
CB-Control [C]
[c]
CB-Control
[D]
CB-treated with Cu(II), Cd(II), Pb(II)
[d]
CB-treated with Cu(II), Cd(II), Pb(II)
Counts
keV

**Figure 2:**

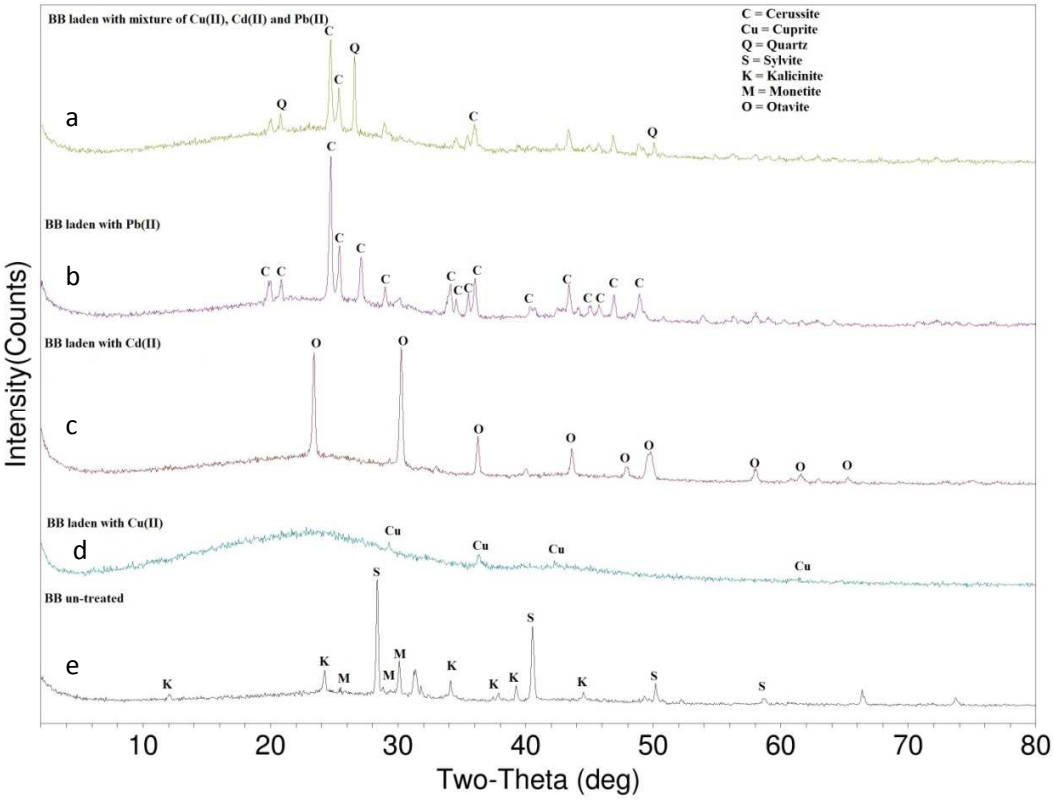
BB laden with mixture of Cu(II), Cd(II) and Pb(II)
C = Cerussite
Cu = Cuprite
Q = Quartz
S = Sylvite
K = Kalicinite
M = Monetite
O = Otavite
a
BB laden with Pb(II)
b
BB laden with Cd(II)
c
BB laden with Cu(II)
d
BB un-treated
e
Intensity(Counts)
Two-Theta (deg)

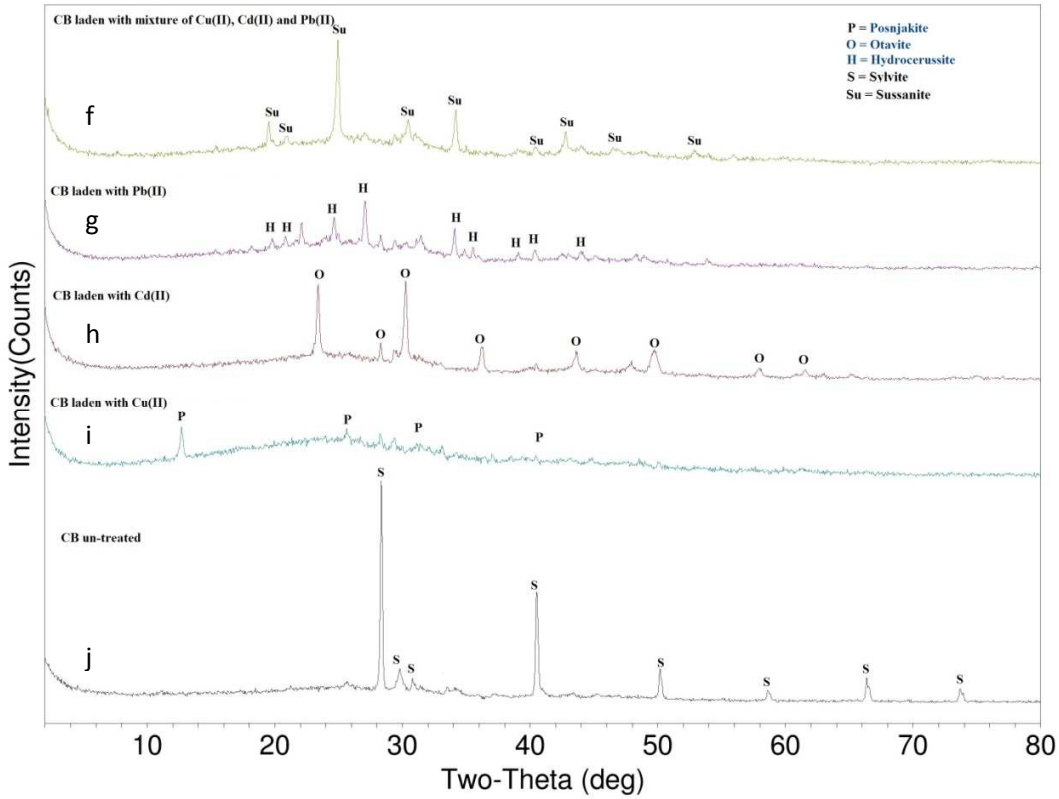
CB laden with mixture of Cu(II), Cd(II) and Pb(II)
P = Posnjakite
O = Otavite
H = Hydrocerussite
S = Sylvite
Su = Sussanite
f
CB laden with Pb(II)
g
CB laden with Cd(II)
h
CB laden with Cu(II)
i
CB un-treated
j
Intensity(Counts)
Two-Theta (deg)

**Figure 3.**

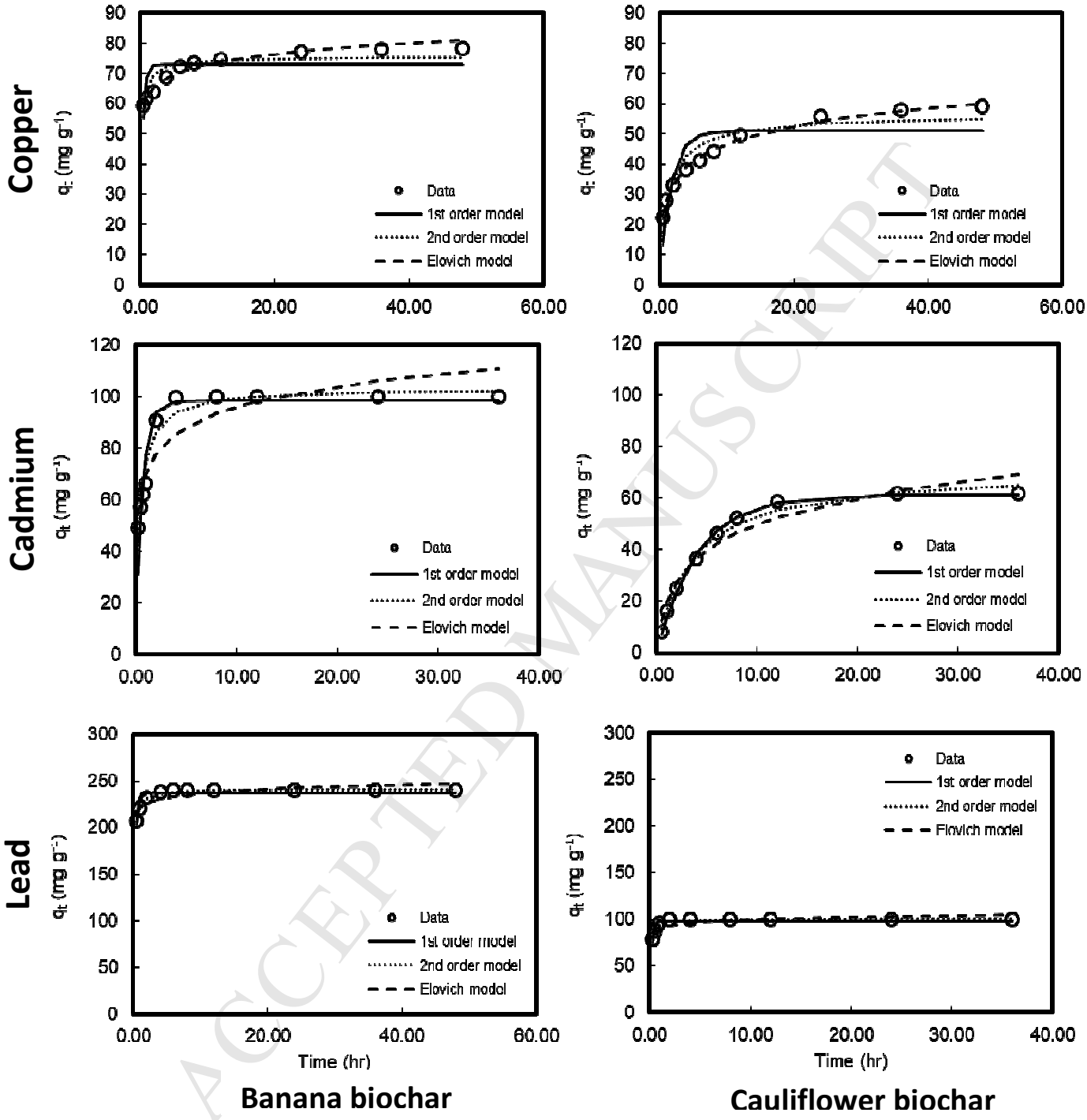

**Figure 4.**

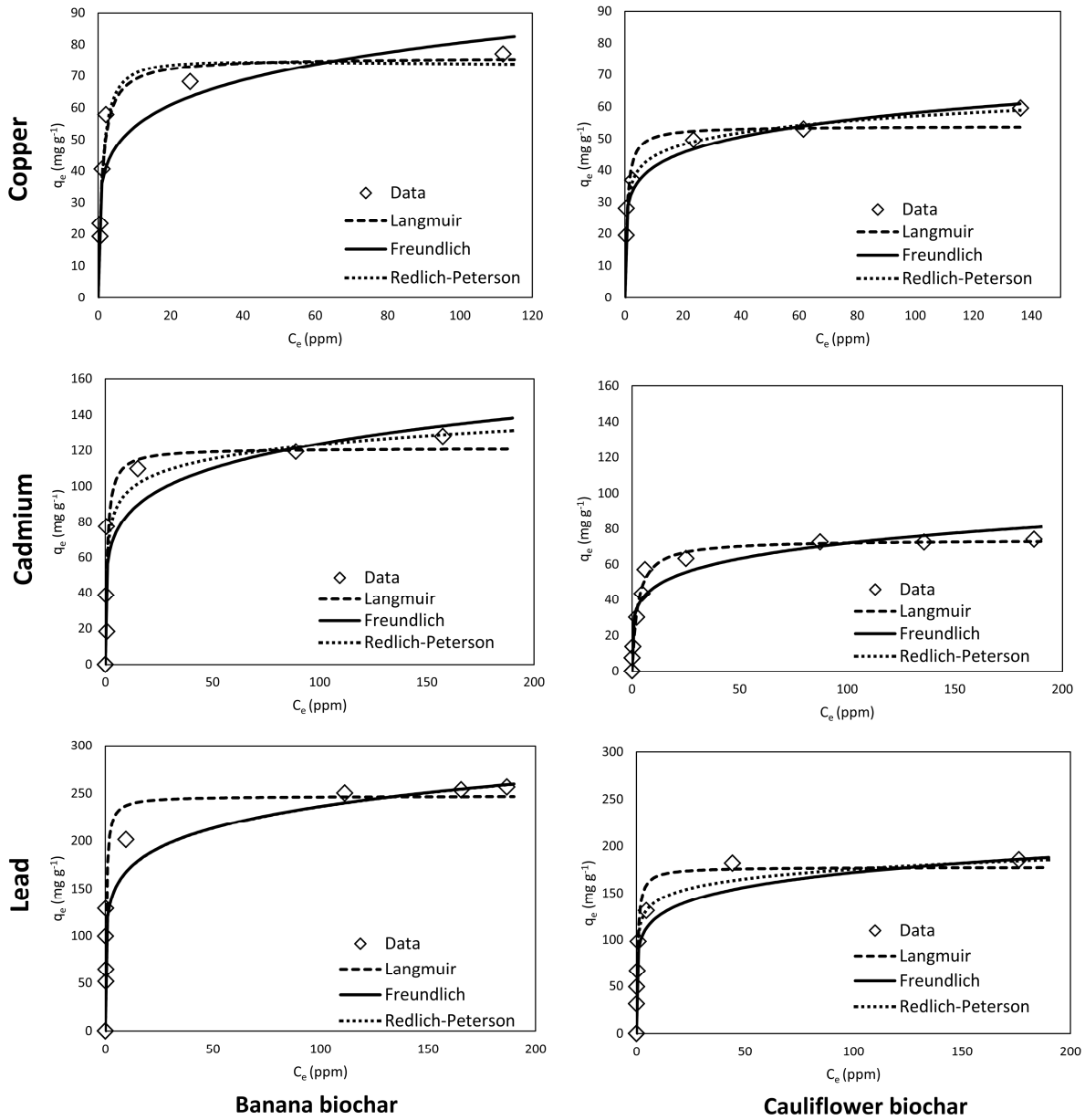
Copper
Cadmium
Lead
$q_e$ (mg g$^{-1}$)
$C_e$ (ppm)
Data
Langmuir
Freundlich
Redlich-Peterson
Banana biochar
Cauliflower biochar

**Figure 5.**

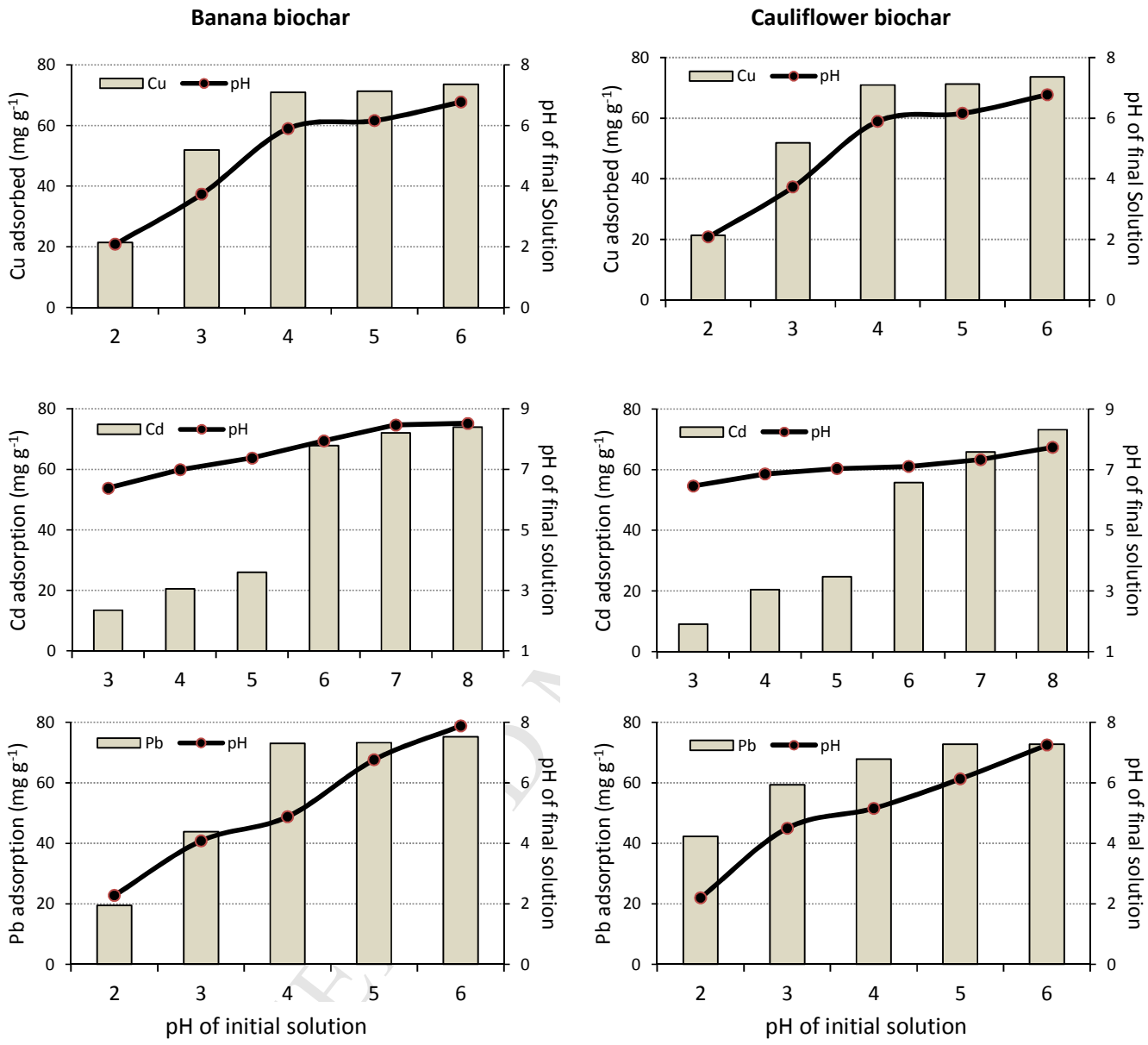
Banana biochar
Cauliflower biochar
Cu
pH
Cu adsorbed (mg g-1)
pH of final Solution
Cd
Cd adsorption (mg g-1)
pH of final solution
Pb
Pb adsorption (mg g-1)
pH of initial solution

**Figure 6.**

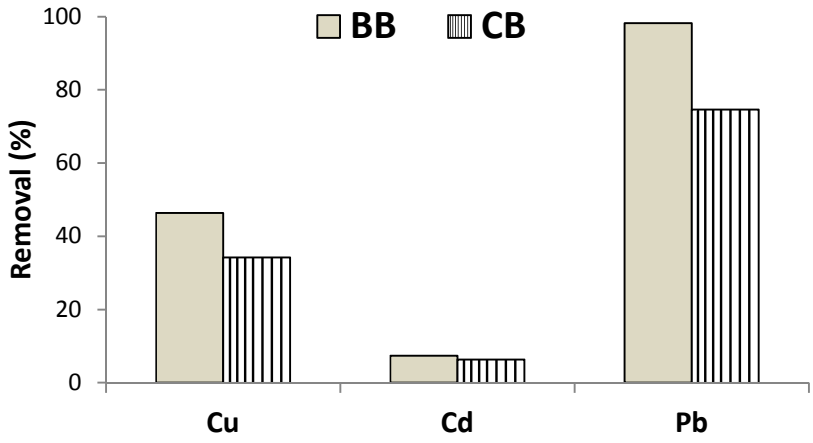

Title: Removal of Cu(II), Cd(II) and Pb(II) ions from aqueous solutions by biochars derived from potassium-rich biomass

**Highlights**

1. The XRD patterns showed the excellent crystallinity of both banana peel biochar (BB) and cauliflower leaves biochar (CB).
2. Apparent sorption of heavy metals was rapid during the first 5-10 h, and the equilibrium was reached at 24 h.
3. Pseudo-second-order was the best model describing the sorption of Pb(II) and Cd(II) onto both biochars ($R^2 > 0.94$)
4. Sorption capacity ($S_{max}$) of heavy metal was higher in BB as compared to other biochar reported in literature.